Combined impacts of climate change and human activities on blue and green water resources in the high-intensity development watershed

Xuejin Tan [1], Bingjun Liu [2*], Xuezhi Tan [2, 3*], Zeqin Huang[2], Jianyu Fu[2]

[1] School of Geography and Planning, Sun Yat-sen University, Guangzhou, 510006, PR China

[2] Center of Water Resources and Environment, School of Civil Engineering, Sun Yat-sen University, Guangzhou, 510275, PR China

[3] Southern Marine Science and Engineering Guangdong Laboratory (Zhuhai), Sun Yat-sen University, Zhuhai, 519082, PR China

* Corresponding authors: Bingjun Liu (liubj@mail.sysu.edu.cn)

Xuezhi Tan (tanxuezhi@mail.sysu.edu.cn)

Abstract

Sustainable management of blue and green water resources is vital for the stability and sustainability of watershed ecosystems. Although there has been extensive attention to blue water (*BW*) which is closely related to human beings, the relevance of green water (*GW*) for ecosystem security is typically disregarded in water resource evaluations. Specifically, comprehensive studies are scarce on the detection and attribution of variations of blue and green water in the Dongjiang River Basin (DRB), an important source of regional water supply in the Guangdong-Hong Kong-Macao Greater Bay Area (GBA) of China. Here we assess the variations of *BW* and *GW* scarcity, and quantify the impacts of climate change and land use change on *BW* and *GW* in DRB using a multi-water-flux calibrated Soil and Water Assessment Tool (SWAT). Results show that *BW* and green water storage (*GWS*) in DRB increased slowly with a rate of 0.14 and 0.015 mm a^{-1}, respectively, while green water flow (*GWF*) decreased significantly at a rate of -0.21 mm a^{-1}. The degree of *BW* and *GW* scarcity in DRB is low, and the per capita water resources in more than 80% of DRB exceed 1700 m^3 $capita^{-1}$ a^{-1}. Attribution results show that 88.0%, 88.5%, and 39.4% of changes in *BW*, *GWF*, and *GW*S result from climate change, respectively. Both climate change and land use change have decreased *BW*, while climate change (land use change) have decreased (increased) *GWF* in DRB. These findings can guide the optimization of the allocation of blue and green water resources between upper and lower reach areas in DRB and further improve the understanding of blue and green water evolution patterns in humid regions.

Key words: Blue and green water; Water scarcity; Climate change, Land use change; Water flow; Dongjiang River Basin

1 Introduction

Land use and land cover change (LUCC), and climate variability may alter hydrological processes in watersheds (Berezovskaya et al., 2004; Chagas et al., 2022; Konapala et al., 2020; Xuezhi Tan et al., 2022), which successively affect variations of regional water resources (Hoek van Dijke et al., 2022; Pokhrel et al., 2021; Stocker et al., 2023; Suzuki et al., 2021), potentially leading to ecosystem degradation and severe water shortage crises (Aghakhani Afshar et al., 2018; Zuo et al., 2015). With the development of society and the economy, there is an increasing need of water resources to accommodate human water utilization, encompassing agricultural, domestic, and industrial water usage. Water scarcity and spatiotemporal mismatch between regional water supply and demand in certain regions are becoming increasingly severe, significantly affecting sustainable development in these regions (Cook et al., 2014). Quantifying water resources in a changing environment is crucial for guiding efficient and sustainable water use.

Previous studies on water resource assessment have explored the effects of climate change and anthropogenic factors on available water resources, including streamflow (Tan and Gan, 2015; Tan et al., 2023; Xin et al., 2019), baseflow (Ficklin et al., 2016; Tan et al., 2020), lake water (Acero Triana and Ajami, 2022; Tao et al., 2020), and groundwater (Han et al., 2020). Falkenmark and Rockström (2006) introduce a novel perspective on water resource assessment by categorizing water resources into BW and GW. BW is the total of deep aquifer recharge and river streamflow, such as water in lakes and rivers. Water users such as industries, agriculture, and municipal users can directly utilize BW. On the contrary, GW is the portion of precipitation that is not drained to river for streamflow generation. GW is temporarily retained in the soil before eventually being released back into the air by evapotranspiration. GW encompasses both green water flow (GWF) and green water storage (GWS) (Veettil and Mishra, 2018; Zang and Liu, 2013). Traditional water resource assessments concentrate on available water resources and only consider BW, but neglect GW (Dai et al., 2022), although GW is also essential. GW supplies about 80% of total water resources, sustaining crop growth and the sustainable development of forest and grassland ecosystems in arid regions or during dry seasons (Li et al., 2018; Schuol et al., 2008). Green water scarcity can lead to ecosystem degradation and intensify competition between human needs and ecosystems for water resources (Falkenmark et al., 2003; Veettil and Mishra, 2018). Compared to traditional streamflow assessment methods, water resource scarcity assessment methods based on the framework of BW and GW are more appropriate for maintaining sustainable water resource management (Cooper et al., 2022; Liu et al., 2017). Recently, some studies have characterized water scarcity by assessing variations of BW and GW. For example, Veettil and Mishra (2020) assess blue water scarcity and green water scarcity to show the water security status of counties in the United States. Hoekstra et al. (2012) use the concept of BW footprint to study water scarcity issues. Schyns et al. (2019) use the GW footprint to investigate green water scarcity and find that the increasingly severe shortage of GW poses a significant threat to natural ecosystems.

The impacts of climate change and anthropogenic on the hydrological cycle processes in watersheds have attracted widespread attention (Chouchane et al., 2020; Cooper et al., 2022; Sherwood and Fu, 2014; Tan and Gan, 2015; Xuejin Tan et al., 2022; Veettil and Mishra, 2016).

Changes in land use alter the underlying surface conditions. For example, afforestation or deforestation may exacerbate or alleviate global or regional climate change, and thus affect hydrological cycle processes (Bai et al., 2020; Lian et al., 2020; Qiu et al., 2023). Changes in land use often lead to alterations in land-atmosphere interactions, and vegetation cover changes are essential for regulating climate systems and land ecosystems (Foley et al., 2005; Huang et al., 2020). Large-scale greening could modify geophysical interactions between the atmosphere and the ground, impacting larger or local regional hydrological cycles. Land degradation (Walters and Babbar-Sebens, 2016), deforestation (Lee et al., 2011), and urbanization (Mohan and Kandya, 2015; Zhang et al., 2018) also have far-reaching effects on the climate and hydrological cycle.

Climate change is also crucial to the variations in BW and GW resources. Precipitation is the source of BW and GW, and factors such as temperature, solar radiation, and potential evapotranspiration significantly influence the changes of BW and GW in watersheds, especially in GWF (Pandey et al., 2019; Schewe et al., 2014). For a single watershed, BW depends directly on precipitation and evapotranspiration (GWF) (Shen et al., 2017; Vano et al., 2012). Furthermore, precipitation intensity can have a significant impact on the redistribution of precipitation, BW, and GW, by altering infiltration and runoff generation processes (Eekhout et al., 2018; Nearing et al., 2005). Therefore, it is crucial to quantify the effects of climate change and LUCC on BW and GW resources in a watershed for effective water resource planning and management.

Water resources management is the primary issue to be addressed for water security.

Hydrological models are important tools to meet various needs in water resource management. Hydrological model simulation is an effective method to evaluate changes in blue and green water resources. As a widely used semi-distributed parametric hydrological model, the SWAT model, which typically subdivides watershed into smaller subbasins, is increasingly used in water resources management at the watershed scale. Based on the SWAT model, researchers simulated the spatiotemporal changes in blue and green water resources in Iran (Jeyrani et al., 2021), the Yangtze River basin (Nie et al., 2023), the Poyang Lake basin (Liu et al., 2023), India (Sharma et al., 2023). Some studies have also used model simulations to analyze the effects of climate change and human activities on water resource changes in Meki River basin (Hordofa et al., 2023), China (Liu et al., 2022), and Ningxia (Wu et al., 2021), etc. However, most of the hydrological models used in the study were calibrated and validated using only observed streamflow data without checking the accuracy of other simulated water variables, which can lead to uncertainties in modeling soil moisture and evapotranspiration (Nie et al., 2023).

The Dongjiang River Basin (DRB) is a crucial water source region for core cities in GBA, such as Shenzhen, Hong Kong, and Huizhou. Given the significant BW demand from agriculture, domestic utilization, and industry, as well as the GW demand from over 18,000 km^2 of forested land, the water resource stress in DRB is extremely high, although DRB is located in the wet South China (Liu et al., 2018). The growing mismatch between increasing water demand and decreasing water supply, along with seasonal and pollution-induced water scarcity issues, is becoming increasingly prominent (Yang et al., 2018). However, the majority of current studies on water resources of DRB focus on changes and scarcity of surface water and groundwater (*BW*) while overlooking the critical role and spatiotemporal variations of *GW* (Huang et al., 2022; Jiang et al., 2023; Jiefeng Wu et al., 2021). With the high-intensity urbanization and climate change in DRB, changes of *BW* and *GW* resources in DRB remain unknown.

This research aims to analyze the influence of climate change and LUCC on *BW* and *GW* in DRB. The objectives of this research are (a) to build the SWAT model for DRB hydrological simulation, (b) to quantitatively evaluate the spatial and temporal variation of *BW* and *GW* in DRB, (c) to assess the status of water scarcity in DRB using the framework of *BW* and *GW* resources, and (d) to estimate the effects of climate change and LUCC on *BW* and *GW* in DRB.

2 Materials and methods

2.1 Study area

The Dongjiang River is an important tributary of the Pearl River, positioned between longitude 113°25'-115°52'E and latitude 22°26'-25°12'N. It originates in Xunwu County, Jiangxi Province, flows through Jiangxi and Guangdong provinces, and goes across major cities including Longchuan, Heyuan, Dongguan, and Shenzhen. The trunk stream of the Dongjiang River has a total length of 562 km. DRB covers a watershed area of 3.5×104 km^2. DRB is of the subtropical monsoon climate zone with adequate precipitation and high temperatures. The average annual precipitation ranges from 1500-2400 mm, and the average temperature of the basin is 21℃ (Wu et al., 2019). The altitude of the basin decreases from the northeast to the southwest. Regions of the upper reaches of DRB are dominated by mountains and hills, those of the middle reaches of DRB are dominated by hills and plains, and those of the lower reaches of DRB are dominated by plains.

Previous hydrological simulation studies of DRB mainly use the Boluo hydrometric station as the outlet of the watershed (He et al., 2013; Jiefeng Wu et al., 2019), so this research only analyze the area of DRB where water flows to the Boluo station (Fig. 1). The Boluo hydrometric station is the main control station in the lower reaches of the Dongjiang. The Boluo hydrometric station occupies a drainage area of 25,325 km^2, which is 71.7% of the total area of DRB. Since the 1950s, more than 896 reservoirs, ponds, dams, and other water conservancy facilities have been constructed in DRB. Among them, the Baipenzhu Reservoir, Fengshuiba Reservoir, and Xinfengjiang Reservoir are the three largest reservoirs in the basin with a cumulative storage capacity of 17,048 million m^3. The Dongjiang-Shenzhen Water Supply Project constructed in 1964 diverts water from the Dongjiang River to Shenzhen and Hong Kong for providing fresh water resources for municipal use. Over 70% of Hong Kong's freshwater supply comes from the Dongjiang River. Therefore, it is crucial to comprehend the shifts in water resources within DRB for projecting future available water resources for the development of GBA.

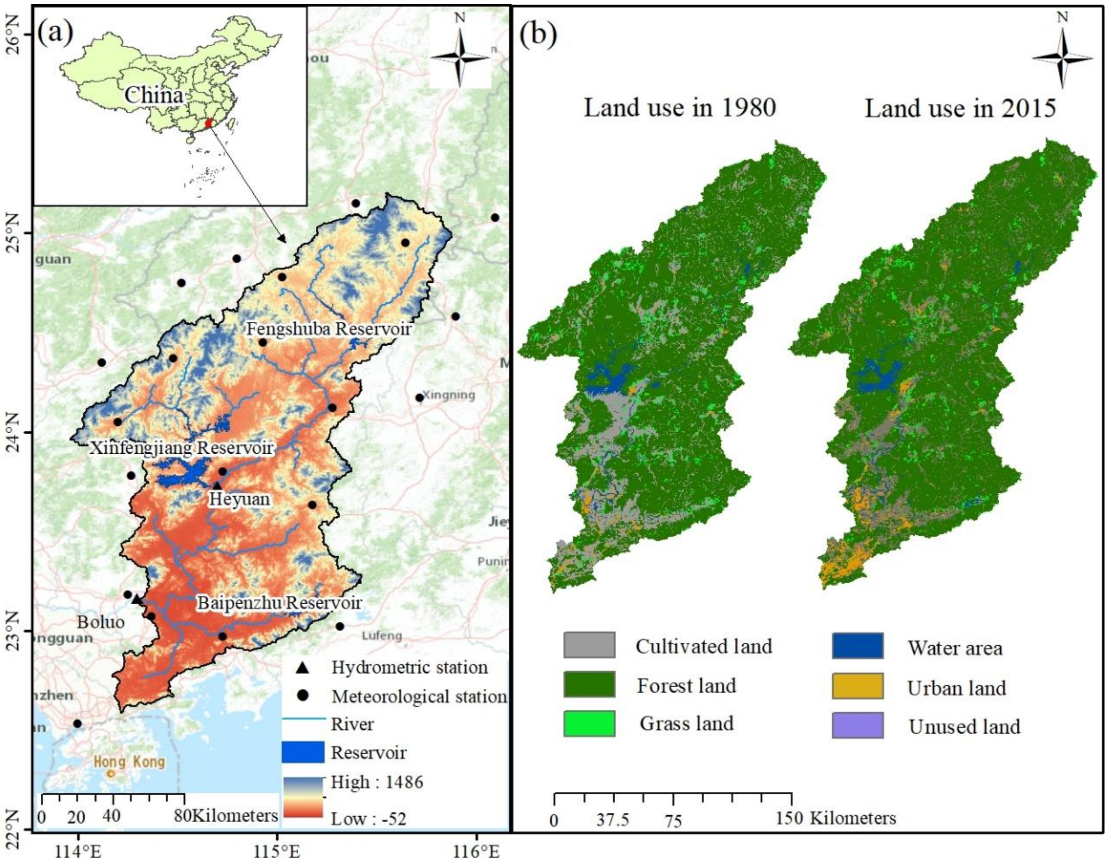

Figure 1. Location and characteristics of the study area: (a) location of the watershed, spatial distribution of the hydrometeorological stations, and digital elevation model (Farr et al., 2007), (b) land use map (Xu et al., 2018).

2.2 Methodology

2.2.1 SWAT model

The SWAT model was adopted to simulate hydrological processes and estimate the amount of *BW* and *GW* for DRB (Arnold et al., 1998; Neitsch et al., 2002). The SWAT model is widely applied to simulate streamflow and surface runoff (Arshad et al., 2022; Martínez-Salvador and Conesa-García, 2020; Nie et al., 2023). The SWAT model is also widely utilized for exploring changes in *BW* and *GW* (Dai et al., 2022; Liang et al., 2018; Schuol et al., 2008).

In SWAT modeling, DRB was divided into 63 sub-basins (Fig. S1), and each sub-basin was then categorized into Hydrologic Response Units (HRUs) depending on land use, soils, and slope.

2.2.2 Model calibration and validation

In order to reduce the influence of hydraulic engineering, the SWAT model was calibrated and validated by utilizing monthly restored natural streamflow at the Boluo and Heyuan hydrometric stations. The optimum model parameters are shown in Table 1. All the selected parameters are automatically calibrated with 500 simulations via SWAT-CUP. The warm-up period for model simulations is the first two years of the simulation period. Reconstructed natural streamflow in 1970-1979 was used to calibrate the model, and monthly time series of reconstructed natural streamflow, *ET* from GLEAM, and soil moisture data from ERA5 during 1980-1989 were used to validate the model. The calibration period for this research was 1970-1979, and the validation period was 1980-1989. Three metrics, including the determination coefficient (R^2), the percentage bias (*PBIAS*), and Nash-Sutcliffe efficiency (*NSE*) were applied to evaluate the simulation performance of the SWAT model:

$$NSE = 1 - \frac{\sum_{i=1}^{n}(Q_{nat} - Q_{sim})^2}{\sum_{i=1}^{n}(Q_{nat} - Q_{ave})^2} \tag{1}$$

$$PBIAS = \frac{\overline{Q_{sim}} - Q_{ave}}{Q_{ave}} \times 100 \tag{2}$$

$$R^2 = [\frac{\sum_{i=1}^{n}(Q_{nat} - Q_{ave})(Q_{sim} - \overline{Q_{sim}})}{\sqrt{\sum_{i=1}^{n}(Q_{nat} - Q_{ave})^2 \sum_{i=1}^{n}(Q_{sim} - \overline{Q_{sim}})}}]^2 \tag{3}$$

where Q_{nat}, Q_{ave}, Q_{sim}, and $\overline{Q_{sim}}$ are monthly natural streamflow, mean monthly natural streamflow, simulated streamflow, and mean monthly simulated streamflow, respectively. n is the total number of time step.

Table 1 Range of the main parameters and their optimal values obtained from the model calibration

Parameter	Calibration type	Initial range	Best calibrated value
GW_REVAP.gw	V	0.19-0.2	0.199
GWQMN.gw	V	493-1247	916.493
SLSUBBSN.hru	R	2.6-5.7	2.804
ESCO.hru	V	0.89-0.97	0.901
CN2.mgt	R	0.14-0.27	0.209
CH_K2.rte	V	0.38-1.16	0.926
ALPHA_BNK.rte	V	0.12-0.18	0.165
SOL_AWC.sol	R	0.3-0.6	0.598
SOL_K.sol	R	0.32-0.69	0.669
CH_K1.sub	V	0-0.15	0.0295

Note: The symbols of V and R denote a replacement and a relative change to the default parameter value, respectively.

This study reconstructed the natural monthly streamflow series of the basin by combining the inflow and outflow of the three major reservoirs (Xinfengjiang Reservoir, Fengshuba Reservoir, and Baipenzhu Reservoir) in DRB, based on the watershed water balance (Tu et al., 2018):

$$Q_{nat} = Q_o + \Delta Q = Q_o + Q_{in} - Q_{out} \tag{4}$$

where ΔQ is the total reduced water volume, Q_o, Q_{in}, and Q_{out} are the observed streamflow, reservoir inflow, and reservoir outflow, respectively.

2.3 Calculation of blue and green water and water security indicators

2.3.1 Calculation of blue and green water

BW is calculated from the sum of water yield (SWAT output WYLD) and groundwater storage. The former refers to the amount of water that leaves the HRU and enters the channel. The latter represents the net amount of water recharged to aquifers (SWAT output GW_RCHG) and the amount of aquifer water discharges to the main channel (SWAT output GW_W) during a time step (Hordofa et al., 2023). *GW* can be divided into two components including *GWF* which is the actual evapotranspiration (SWAT output ET) from the HRU, and *GWS* which is the soil water moisture (SWAT output SW) (Nie et al., 2023; Veettil and Mishra, 2018). The calculation of the Green Water Index (*GWI*) involves dividing the quantity of *GW* by the sum of *BW* and *GW* (Ding et al., 2024; Nie et al., 2023).

2.3.2 Blue and green water scarcity

Blue water scarcity (*BWSC*) is determined by the quotient of *BW* withdrawal and availability. The estimation of *BW* withdrawals (*BWW*) in this study involved the multiplication of the aggregate population in each sub-basin by the combined water consumption per person (Liang et al., 2020). The population of each sub-basin was extracted from the population raster data. Blue water availability (*BWA*) represents the quantity of water that can be utilized without negatively impacting the river ecosystems. Exhaustive exploitation of *BW* in rivers may adversely impacts river ecosystems. Previous studies have generally used environmental flow requirements (*EFR*) as a suitable metric for sustaining robust ecosystems (Honrado et al., 2013). According to the study of Richter (2010) and Richter et al. (2012), extracting more than 20% of the water from rivers may result in ecological degradation. Therefore, 20% of streamflow can be deemed *BW* and used for water supply (Veettil and Mishra, 2016). The calculation of *EFR*, *BWA*, and *BWSC* are as follows:

$$EFR_{(a,t)}=0.8\times Q_{\text{mean}(a,t)} \tag{6}$$

where $EFR_{(a,t)}$ is the *EFR* for sub-basin '*a*' during time '*t*'; Q_{mean} is the long-term monthly average streamflow.

$$BWA_{(a,t)} = Q_{(a,t)} - EFQ_{(a,t)} \tag{7}$$

$$BWSC=BWW/BWA \tag{8}$$

Green water scarcity (*GWSC*) is defined as the ratio between green water footprint (*GWFO*) and green water availability (*GWA*). *GWFO* denotes the actual evapotranspiration from the watershed. *GWA* is the soil moisture that is available for evapotranspiration and vegetation transpiration and is equal to the initial soil moisture (Liang et al., 2020). The *GWSC* can be formulated as:

$$GWSC_{(a,t)}=GWFO_{(a,t)}/GWA_{(a,t)} \tag{9}$$

where *GWSC* is green water scarcity; $GWFO_{(x,t)}$ is the actual evapotranspiration; $GWA_{(a,t)}$ is initial soil moisture。

2.3.3 Regional water stress

The Falkenmark index (*FLK*) (Falkenmark et al., 1989) is a widely used measures of water stress, defined as the proportion of *BWA* to the overall population. The Falkenmark index is classified into no stress, stress, scarcity, and absolutely scarcity based on per capita water use. Absolute scarcity is regarded to occur in areas where the indicator threshold is less than 500 m^3 $capita^{-1}$ a^{-1}, and no stress is thought to occur in areas where the threshold is larger than 1700 m^3 $capita^{-1}$ a^{-1}.

2.4 Calculation of relative contribution

2.4.1 Scenario design and simulation

Three scenarios were constructed to assess the impacts of climate change and LUCC on *BW* and *GW* by changing climate conditions (land use) while holding land use (climate conditions) for the three scenarios simulation each (Table 2). The land use map was fixed when simulating the influences of climate change on blue and green water (S2-S1), while climate conditions was fixed when simulating the influences of LUCC on blue and green water (S3-S2). The climate conditions and the land use were altered when assessing the joint influences of climate change and LUCC on blue and green water (S3-S1).

Table 2 Scenario settings for the simulation of effects of climate change and LUCC on blue and green water

Scenarios	Land use	Climate period	Combined effects	Land use change effects	Climate change effects
S1	1980	1970-1993			
S2	1980	1994-2017			S2-S1
S3	2015	1994-2017	S3-S1	S3-S2	

2.4.2 Relative contribution rate calculation

The influences of climate change and LUCC on the changes of blue and green water in different periods are evaluated utilizing the relative contribution (*RC*) in this research (Li et al., 2021):

Climate change contribution to *BW* and *GW* change is estimated by:

$$RC_C = \frac{|X_2 - X_1|}{|X_2 - X_1| + |X_3 - X_2|} \times 100\% \tag{10}$$

where X_1, X_2, and X_3 are the amount of water including BW or GWF and GWS, respectively for scenario S1, S2, and S3.

The contribution of LUCC to changes in BW and GW are estimated by Equations 11.

$$RC_L = \frac{|X_3 - X_2|}{|X_3 - X_2| + |X_2 - X_1|} \times 100\% \tag{11}$$

2.5 Data

The dataset used in this study consists of three parts: (1) hydrometeorological data, (2) geospatial data encompassing DEM, soil type, and land use, and (3) socioeconomic data encompassing per capita water consumption and population data.

Observed monthly streamflow data of the two hydrological stations in the study were collected for the years 1970-2000 from Boluo Station and Heyuan Station, and the observed streamflow time series of these two hydrological stations are of no missing data. Monthly inflow and outflow data of the three major reservoirs in DRB were also collected. All hydrologic data were obtained from the Guangdong Provincial Hydrological Bureau. Meteorological data of daily precipitation, temperature, and other meteorological data for 1968-2017 from 21 Meteorological stations in the watershed were obtained from the National Meteorological Information Center of the China Meteorological Administration. Monthly actual *ET* data for SWAT model validation was obtained from the Amsterdam Evapotranspiration Model dataset with a spatial resolution of 0.25° × 0.25° (Martens et al., 2017). Monthly soil moisture data for SWAT model validation was obtained from the European Center for Medium-Range Weather Forecasts ERA5-land dataset with a spatial resolution of 0.1° × 0.1° (Muñoz Sabater, 2019). The actual evapotranspiration and soil moisture of the watershed equals to the average of all grids included in DRB.

The 90-meter resolution DEM data and 30-meter resolution land use data at ten-year intervals (i.e., 1980, 1990, 2000, 2010, 2015) are obtained from the Data Center for Resources and Environmental Sciences of the Chinese Academy of Sciences (Xu et al., 2018). Soil data is obtained from the 1-km resolution Harmonized World Soil Database dataset from the Food and Agriculture Organization of the United Nations (Fischer et al., 2008).

The annual per capita integrated water consumption data of DRB from 2000-2017 was acquired from the Water Resources Bulletin of Guangdong Province. The population data in 2000, 2005, 2010, and 2015 was obtained from the 1 × 1 km spatial raster data of the Resource and Environment Science and Data Center of the Chinese Academy of Sciences (Xu, 2017).

3 Results

3.1 Model Performance

The SWAT model shows sufficient accuracies in simulating streamflow, actual evapotranspiration, and soil moisture changes in DRB and can better simulate both seasonal and interannual changes in streamflow. During the calibration period, both stations achieved R^2 above 0.9, *NSE* exceeding 0.8, and *PBIAS* less than 14% (Fig. 2). Both stations had simulated streamflow R^2 greater than 0.8 during the validation period. The *NSE* for streamflow simulation at the Heyuan station and Boluo station of the validation were 0.81 and 0.74, respectively. The model performs well in simulating the *ET* and soil moisture. Since the GLEAM *ET* data and ERA5 soil moisture data are raster data of spatial resolution of 0.25×0.25°, considering the influence of data accuracy on the results, this study uses the watershed scale to validate the simulation results of *ET* and soil moisture. In the validation period, the R^2 and *NSE* for the simulation of evapotranspiration were 0.92 and 0.8, respectively (Fig. S2), while the R^2 and the *NSE* for the soil moisture simulation were both greater than 0.6. These validation results show that the model can be used to simulate hydrological regimes in DRB.

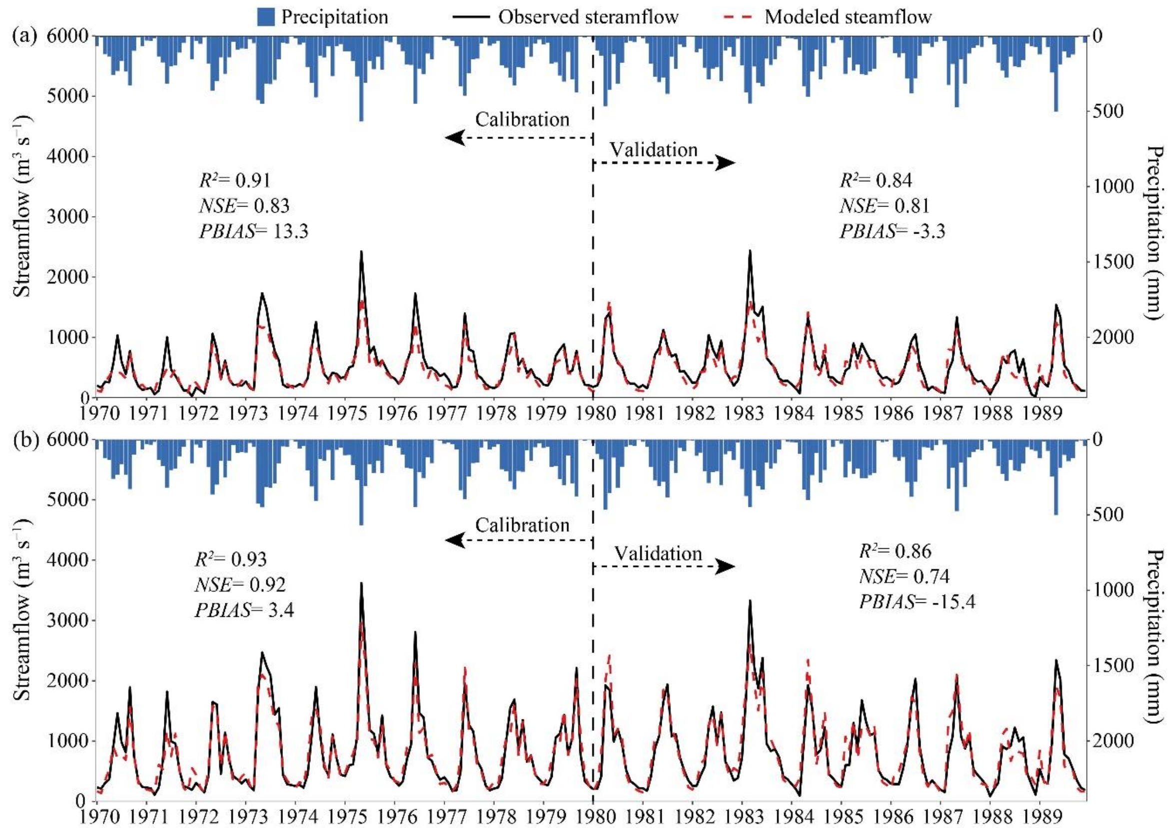

Figure 2. Simulated and observed monthly streamflow at the (a) Heyuan and (b) Boluo gauge stations during calibration and validation periods.

3.2 LUCC and Climate variability in DRB

LUCC in DRB is mainly the decrease of cultivated land and the increase of urban land. The land use in DRB primarily consisted of forest land (18,875-18833 km^2), which is more than 70% of DRB. From 1980 to 2015, the urban land and water areas showed an increase of 469.4 km^2 (137%) and 17.4 km^2 (2.8%), while the grassland, cultivated land, and forest land showed a decrease of 41.3 (4.3%), 487.5 (10.8%), and 42.1 km^2 (0.2%), respectively (Table 3).

Table 3 Land use transfer matrix in DRB from 1980 to 2015

Land use type		2015						1980 total (km^2)
		Grass Land (km^2)	Urban land (km^2)	Cultivated Land (km^2)	Forest land (km^2)	Water area (km^2)	Unused land (km^2)	
1980	Grassland	795.6	29.9	18.3	123.5	2.5	0.0	969.7
	Urban land	0.6	319.6	12.4	7.6	2.3	0.0	342.4
	Cultivated land	19.0	269.8	3771.7	427.9	40.4	0.03	4528.8
	Forest land	110.7	183.7	226.2	18278.7	33.1	0.02	18832.5
	Water area	2.5	8.9	12.7	36.8	551.0	0.00	611.9
	Unused land	0.0	0.0	0.02	0.03	0.00	0.45	0.51
2015 total		928.4	811.9	4041.3	18874.5	629.2	0.51	25285.8

DRB exhibited significant regional differences in multi-year average precipitation, temperature, and potential evapotranspiration. The precipitation exhibited an increasing trend from the central to the south and north of DRB. The temperature and potential evapotranspiration showed an overall distribution pattern of greater values in the south and minor values in the north of DRB (Fig. 3). The multi-year average precipitation for the entire DRB was 1790.1 mm, with annual precipitation ranging from 1236.2-2567.5 mm. The regions with the highest multi-year average annual precipitation are located in the southeast of DRB, where annual precipitation exceeds 2200 mm, while the regions with the lowest precipitation are in the northeastern of the watershed. The average annual temperature in DRB ranged from 19.5-21.3 °C, and the average annual potential evapotranspiration ranged from 1101.5-1320.6 mm. The south of DRB is predominantly urban, characterized by the urban heat island effect, while the north of DRB is mountainous with higher elevations, leading to the spatial distribution of temperatures.

The average temperature and potential evapotranspiration at DRB meteorological stations exhibited significant variations, while precipitation showed a relatively minor trend (Fig. 3). Overall, basin-averaged precipitation and potential evapotranspiration showed a non-significant decreasing trend, while temperatures showed a significant increasing trend. There was no significant change trend of precipitation for all stations in DRB (Fig. 3a). Twenty out of 21 meteorological stations in the region showed statistically significant increasing trends in average temperature, indicating a warming trend (Fig. 3b). Nine stations showed a significant decreasing trend in potential evapotranspiration, primarily located in northern DRB (Fig. 3c).

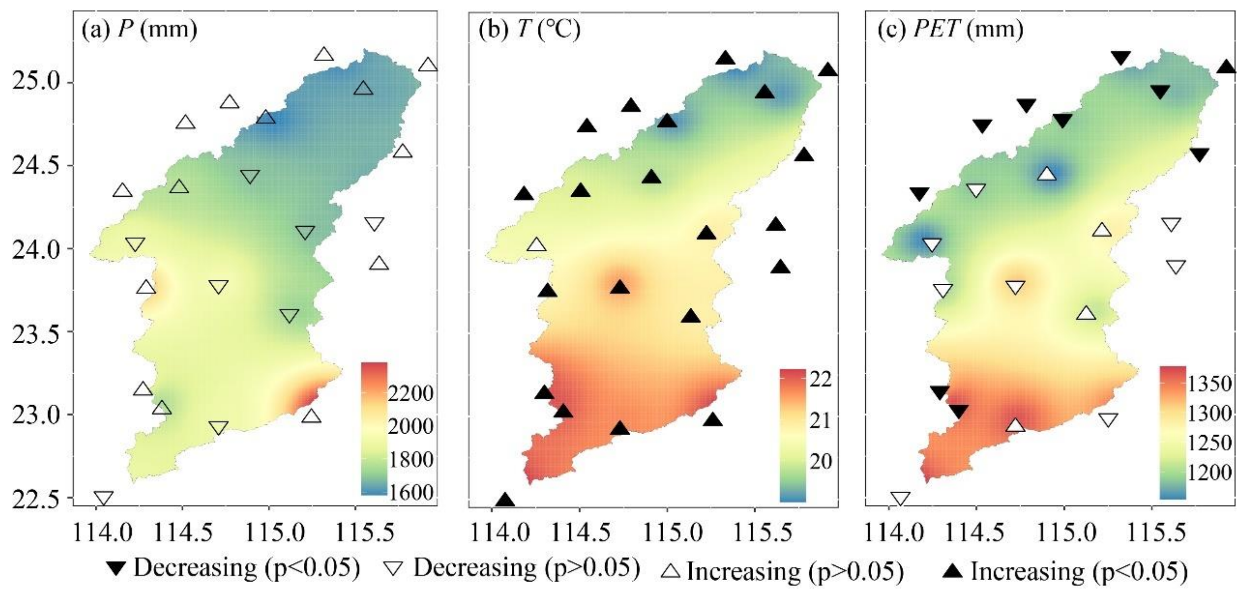

Figure 3. Spatial distribution of annual mean (a) precipitation, (b) temperature, (c) potential evapotranspiration in DRB from 1960-2017. Each triangle represents the Mann-Kendall test result at a meteorological station.

The mean precipitation, temperature, and potential evapotranspiration of DRB can be obtained from the precipitation, temperature, and potential evapotranspiration of stations using the Tyson polygon method. The inter-annual variation of annual precipitation in DRB showed an insignificant decreasing trend (-0.51mm a^{-1}). The annual mean temperature showed a significant increasing trend (0.024°C a^{-1}). The annual potential evapotranspiration showed a significant decreasing trend (-0.38mm a^{-1}) (Fig. S3).

3.3 Blue and green water resources

The average annual *BW* and *GW* were 1240.8 and 840.7 mm, respectively. The DRB water resources were dominated by *BW*, representing 60.1% of the total water resources, and *BW* was 1.48 times higher than that of *GW* resources. The average *GWF* and *GWS* were 689.3 and 151.4 mm, respectively.

The annual *BW* resources in the sub-basins of DRB ranged from 893.7-1990 mm, showing an increasing trend from the central to the south and north of DRB, aligning with the spatial distribution of precipitation (Fig. 4a). The regions with abundant *BW* resources are situated in the central and southeast parts of DRB (>1300 mm), and the *BW* in the upper reaches is comparatively low (<1100 mm). Differences in the spatial distribution of *BW* are primarily caused by differences in the spatial distribution of precipitation. Overall, the *GWF* and *GWS* are more evenly distributed in the sub-basins than *BW*. The annual *GWF* in the sub-basins of DRB ranged from 573.6-923.6 mm. The sub-basins with higher *GWF* are primarily located in the Xinfengjiang reservoir area in the middle reaches (>700 mm), while the low *GWF* sub-basins are situated in the southwest of DRB (<600 mm) (Fig. 4b). The land use in the sub-basins where Xinfengjiang Reservoir is located is primarily water areas, with a higher water evaporation rate than other regions, resulting in a greater *GWF* in this area than in other regions. The annual *GWS* in the sub-basins of DRB ranged from 126-190.6 mm. The sub-basins with higher *GWS* are mainly located in the lower part of DRB (>150 mm) (Fig. 4c). The distribution pattern of *GWS* resources has a great relationship with the soil type of the watershed. The upper reaches and the northwestern part of the watershed are mostly red soil, while the middle and lower reaches are dominated by reddish soil. Reddish soil has a smaller water storage capacity than red soil, loses water faster, and has weaker water conservation and water supply performance than red soil. This is the primary factor for the north-south discrepancies in the amount of *GWS* resources in DRB. In addition, the southern region is mostly of large and medium-sized cities. As urban construction land expands, the land use type in the region has gradually changed to urban land, industrial land, etc., and the solidification of road surfaces has reduced the area of bare soil in the region, resulting in a decrease in *GWS* resources. The annual *GWI* (Fig. 4d) showed a spatial pattern opposite to *BW*, decreasing from 0.45 in the upper reaches to 0.3 in the lower reaches. The highest *GWI* is found in the upper reaches, which is due to the relatively low rainfall in the upper reaches and the lush vegetation, with significant plant interception and transpiration, resulting in a higher proportion of total evapotranspiration than in the middle and lower reaches. The central part of the basin has the highest precipitation, leading to a lower *GWI*. The southern part of the watershed has the highest temperature, and evapotranspiration is high. Meanwhile, the lower reaches have a large proportion of agricultural and urban land, and crop irrigation can increase evapotranspiration.

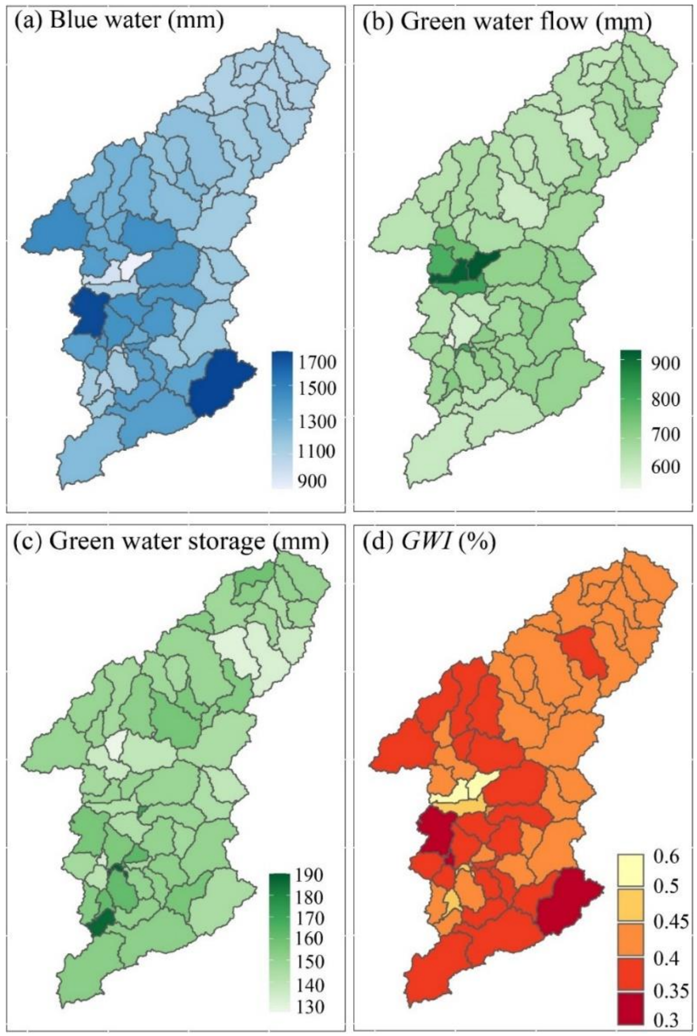

Figure 4. Spatial distribution of mean (a) *BW*, (b) *GWF*, (c) *GWS*, (d) *GWI* in DRB over during 1970-2017.

In DRB, there was no significant increasing trend in either BW or GWS, while GWF exhibited a significant decreasing trend. The annual trend rate of BW in DRB was 0.14 mm a-1, with an annual fluctuation range of 713.6-2017.5 mm during 1970-2017. The minimum BW occurred in 1991, while the maximum was recorded in 2016 (Fig. 5a). The GWF in DRB from 1970 to 2017 exhibited a significant decreasing trend (-0.57 mm a-1) (Fig. 5b). The minimum GWF occurred in 2005 (603.1 mm), while the maximum was recorded in 1974 (721.3 mm). In contrast, the GWS in DRB from 1970 to 2017 has been slowly increasing at a rate of 0.015 mm a-

1 (Fig. 5c). The annual fluctuation in GWS was smaller than BW and GWF. The GWI in DRB from 1970 to 2017 showed no significant decreasing trend at a rate of -0.0003 % a-1 ($p>0.05$) (Fig. 5d), implying that the redistribution of precipitation in DRB might change slowly.

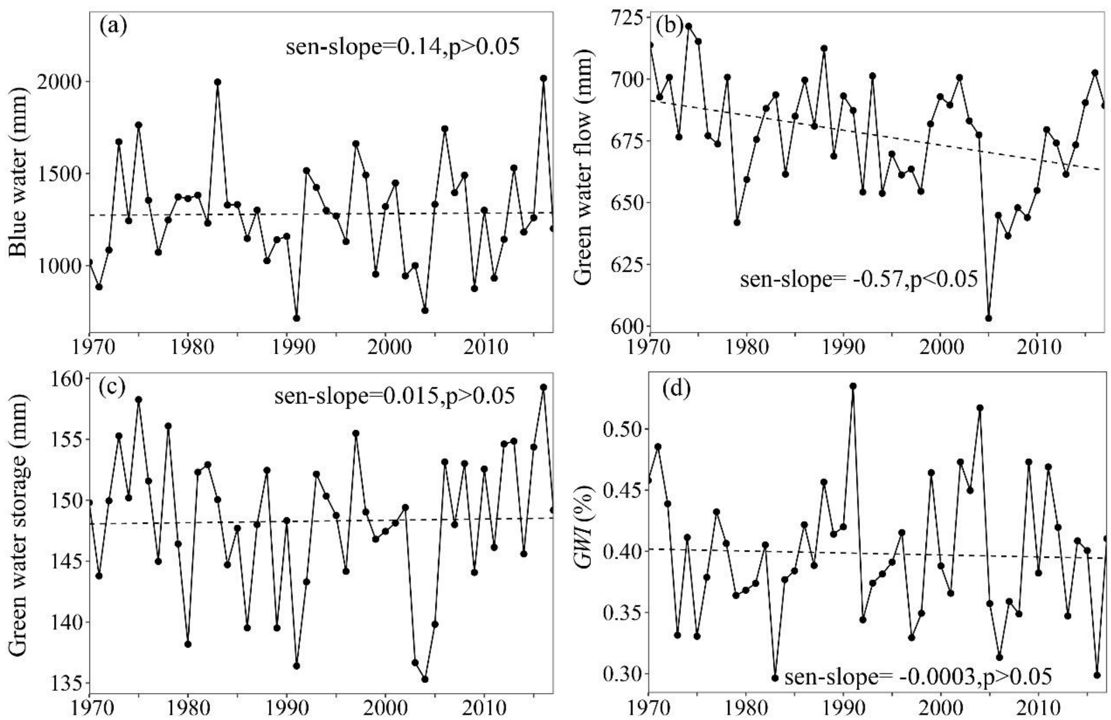

Figure 5. Interannual variation of (a) *BW*, (b) *GWF*, (c) *GWS*, (d) *GWI* in DRB during 1970-2017.

3.4 Blue and green water scarcity

The average blue water scarcity level in DRB was low (22.4%) during 1970-2017. The blue water scarcity levels in various sub-basins ranged from 0.1-206%. The multi-year average blue water scarcity, except for one sub-basin in the southwest, was all low (<100%) (Fig. 6a). This indicates that blue water scarcity is not common in DRB at the annual scale. Regions with relatively high blue water scarcity (>20%) are mostly situated in the upper reaches of various tributaries within the watershed, where river streamflow is relatively small. The area with the highest blue water scarcity (206%) is located in the 63rd sub-basin of Shenzhen and Huizhou, reaching a moderate level of blue water scarcity. This region has a large population, with a much higher blue water demand than other areas. Additionally, this sub-basin is situated in the upper reaches of the primary tributary of DRB, resulting in a limited supply of *BW* resources. Although the northern parts of sub-basins 55, 56, and 61 have large populations, these sub-basins are situated in downstream of the main Dongjiang River, with a higher streamflow, leading to lower *BWSC* levels. The average *GWSC* in the entire basin from 1970-2017 was low (41.4%). The blue water scarcity levels in various sub-basins ranged from 31-104%. The vegetation cover in DRB is high, and DRB is thus of relatively high rates of vegetation transpiration and interception evaporation. The basin experiences a *GWSC* of nearly 50%, indicating a potential occurrence of *GWSC*. The areas with higher *GWSC* are primarily situated in the middle reaches for DRB (Fig. 6b), where water surface evaporation is high, resulting in their *GWSC* exceeding 100%. The evaporated water in these areas originates from the reservoirs, not the soil, leading to an overestimation of the *GWSC* in these sub-basins.

Furthermore, the *FLK* index was also used to quantify population-driven water resource scarcity. F1-F4 represent absolute scarcity, scarcity, stress, and no stress, respectively. The results showed that most regions in DRB have no water scarcity pressure (Fig. 6c). However, the 63rd sub-basin experienced absolute water scarcity, and the 52nd sub-basin experienced water scarcity. There were six lower reaches sub-basins and four upper reaches sub-basins facing water stress.

DRB receives ample precipitation, resulting in a relatively large river flow, generally leading to a higher *FLK* index. As a result, the basin faces lower water resource pressure.

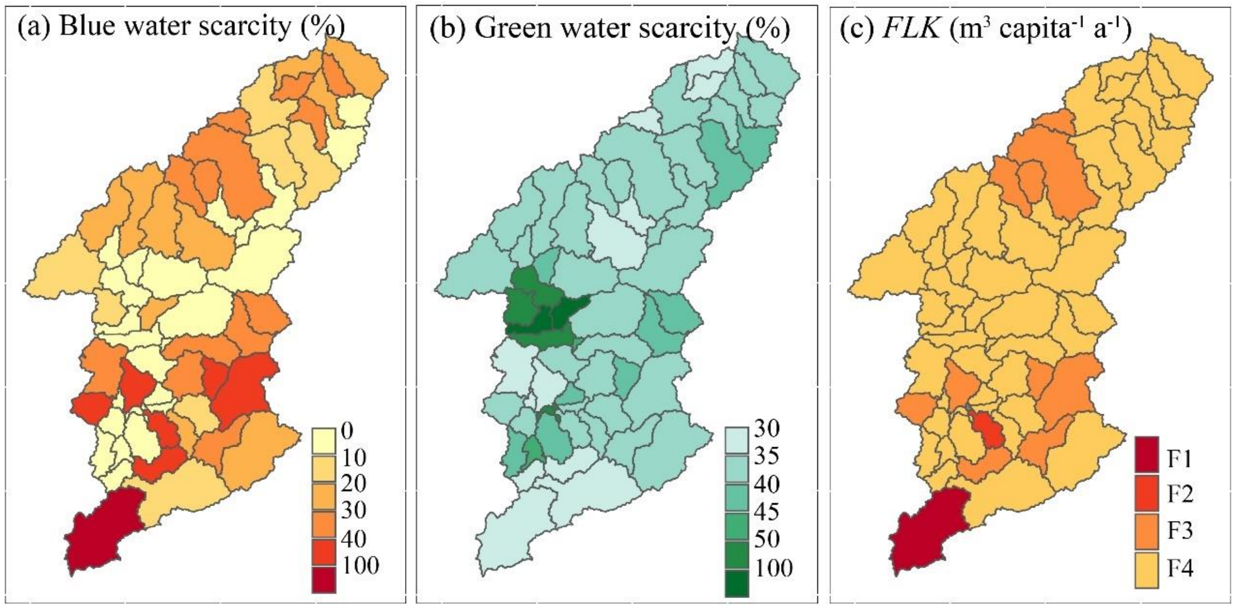

Figure 6. Spatial distribution of mean (a) *BWSC*, (b) *GWSC*, and (c) *FLK* index in DRB over during 1970-2017.

This study also further identified hotspots of *BWSC* and *GWSC* in DRB by hierarchical clustering of *BWSC* and *GWSC* in each sub-basin. Figure 7 shows the clustering tree results for *BWSC* and *GWSC*. When the standardized distance was set to 500, all sub-basins could be divided into four categories according to blue water scarcity: (1) The first category consisted of 27 sub-basins, such as 32, 56, and 28, where the blue water scarcity level was the lowest (<20%). (2) The second category comprised sub-basin 63, which has the most severe blue water scarcity (206%). (3) The third category comprised seven sub-basins, such as 52, 58, and 60, all located in the lower reaches, with relatively high blue water scarcity levels (40%-100%). These sub-basins are mostly located in the tributaries of the lower reaches, with a relatively large population and smaller river streamflow compared to the mainstem of the Dongjiang River. (4) The fourth category consisted of 28 sub-basins, such as 59, 62, and 8, with blue water scarcity levels ranging from 20% to 40%. Similarly, hierarchical clustering was conducted for *GWSC*. When the standardized distance was set to 500, *GWSC* in the sub-basins could be divided into three categories: (1) The first category consisted of 56 sub-basins, such as 37, 56, and 29, with relatively low *GWSC* levels, all below 50%, indicating low *GWSC*. (2) The second category consisted of sub-basins 32 and 33, where the predominant land use type was water areas, leading to higher *GWSC* due to high water surface evaporation. (3) The third category consisted of sub-basins 47, 31, 54, 30, and 36, where the water area proportion in these sub-basins was larger than in others, leading to significant influences from water surface evaporation.

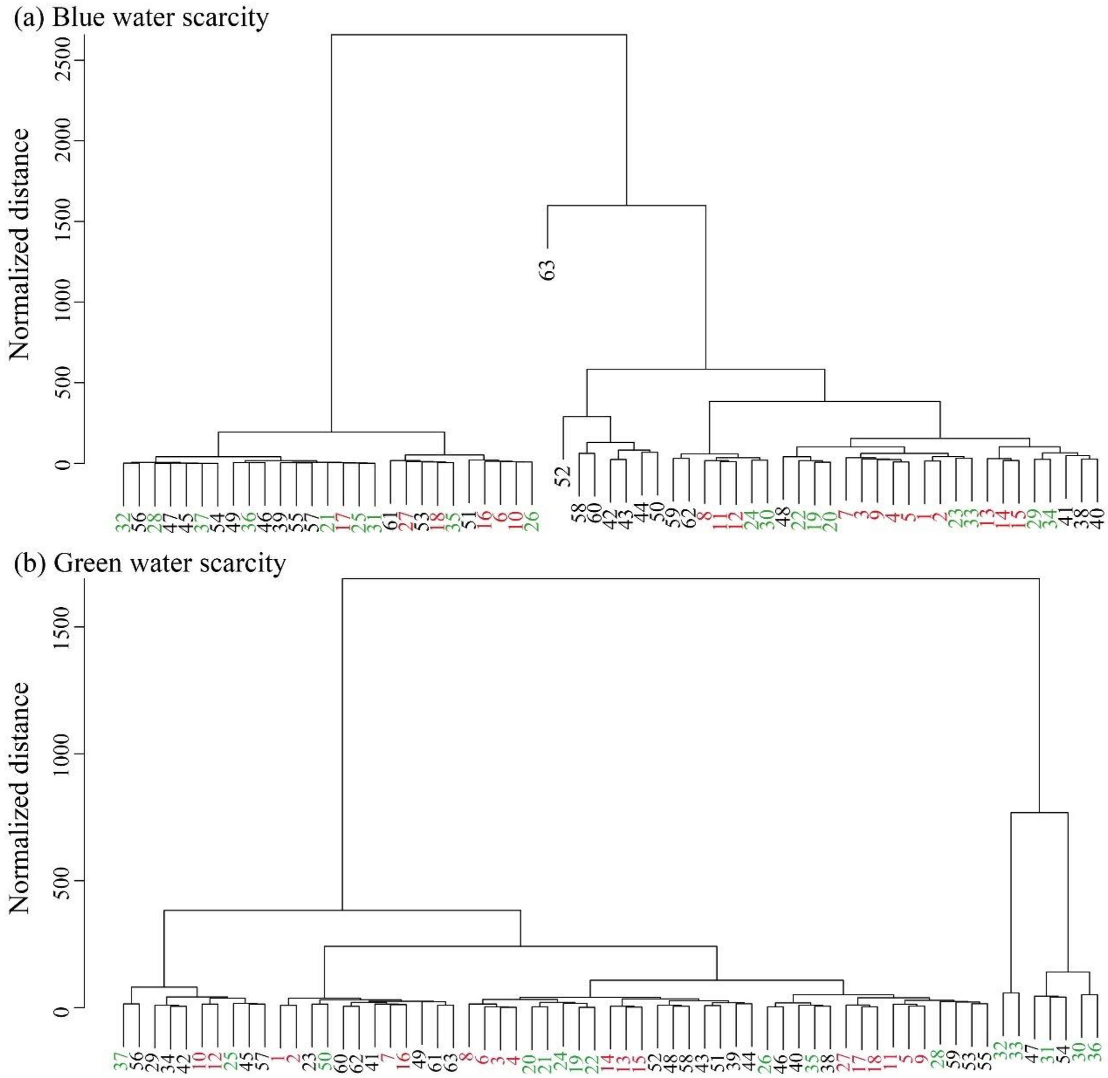

Figure 7. Hierarchical clustering tree of (a) *BWSC*, (b) *GWSC*.

The interannual variations in *BWSC* and *GWSC* in DRB showed distinct regional differences. *BWSC* in the basin was slowly increasing at a rate of 0.3% a^{-1} (Fig. 8a). The *BWSC* in the lower reaches slowly increased at a rate of 1.1 % a^{-1}, while the *BWSC* in the upper and middle reaches slowly decreased at -0.47% a^{-1} and -0.1% a^{-1}, respectively. *GWSC* in the upper, middle, and lower reaches of DRB showed a decreasing trend, with basin scale *GWSC* decreasing significantly at a rate of -0.04% a^{-1} (Fig. 8b). Despite the acceleration of urbanization and a significant increase in population in the middle and lower reaches of the watershed, blue water availability and the amount of obtainable *BW* have been increasing. Additionally, the annual per capita water consumption in the basin has decreased from 481.0 m³ in 2000 to 245.0 m³ in 2020. As a result, the rate of increase in *BWSC* in the watershed has been relatively small. In contrast, the *GWF* in DRB demonstrated a significant decreasing trend, and the *GWS* increased slowly. Therefore, the *GWSC* in DRB demonstrated a significant decreasing trend. Meanwhile, the *FLK* index of the watershed showed a significant decreasing trend (-285.3 m^3 per year), which means that the per capita water resources in the watershed have significantly decreased (Fig. 8c). This is due to the rapid population growth in the watershed and the slow increase in available water resources.

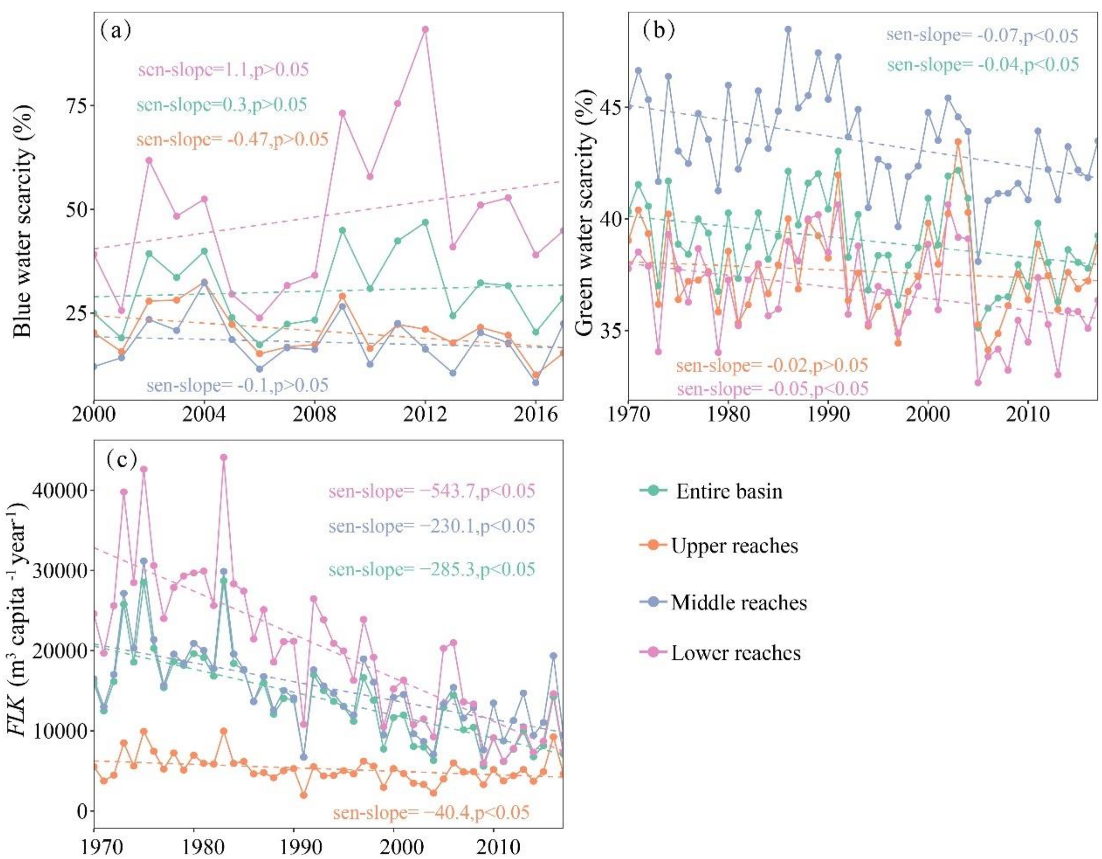

Figure 8. Interannual variation of(a) *BWSC*, (b) *GWSC*, and (c) *FLK* index in DRB during 1970-2017.

3.5 Impacts of LUCC and climate change on blue and green water

To examine the impacts of climate change and LUCC on *BW* and *GW* change, this study set three climate conditions and land use scenarios to explore this effect by comparing the scenarios (Table 3). The combined impacts of climate change and LUCC on *BW* and *GWS* in DRB were superimposed, and the combined effect on *GWF* was a negatively synergistic effect. Figure 6 shows the variations in *BW* and *GW* under the impacts of climate change (S2-S1) and LUCC (S3-S2), as well as their combined effects (S3-S1), along with the relative contribution of climate change and LUCC to the *BW* and *GW* changes in DRB during 1970-2017. Under the joint influences of climate change and LUCC, *BW* decreased by 4.5 mm a^{-1}. Among this decrease, climate change resulted in a loss in *BW* of 3.9 mm a^{-1}, contributing 88.0%, while LUCC led to a loss in *BW* of 0.5 mm a^{-1}, contributing 12.0% (Fig. 9a). The effect of climate change on *BW* variation is much greater than that of LUCC at the basin scale. Under the combined influences of climate change and LUCC, *GWF* decreased by 17.0 mm a^{-1}. Among this decrease, climate change accounted for a decrease in *GWF* of 19.5 mm a^{-1}, contributing 88.5% to the decrease, while LUCC led to an increase in *GWF* of 2.5 mm a^{-1}, contributing 11.5% (Fig. 9b). Overall, the influence of climate change on *GWF* changes in the watershed is significantly more pronounced than that of LUCC. Under the joint influences of climate change and LUCC, *GWS* increased by 0.7 mm a^{-1}. Among this increase, climate change contributed to an increase in *GWS* of 0.3 mm a^{-1}, accounting for 39.4%, while LUCC contributed to an increase in *GWS* of 0.4 mm a^{-1}, accounting for 60.6%

(Fig. 9c). DRB is situated in a humid region with high *GWS*, resulting in small fluctuations of *GWS* in response to precipitation changes. The fluctuations of *GWS* are primarily influenced by soil properties and land use. In general, the effect of climate change on the *GWS* change of DRB is smaller than the effect of LUCC.

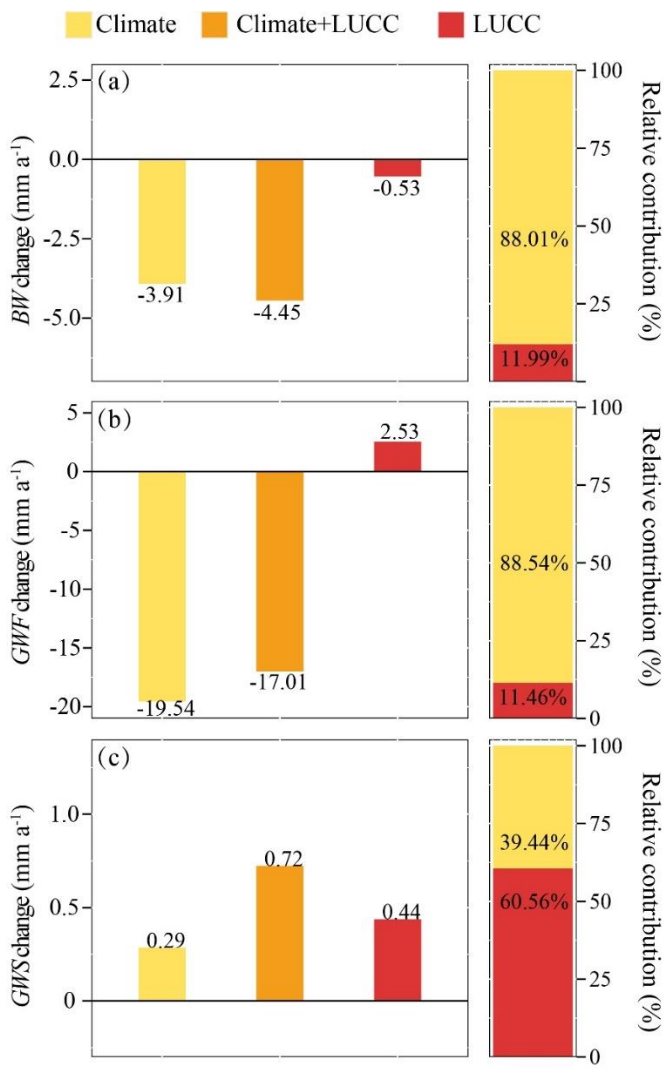

Figure 9. Effects and relative contribution of climate change and LUCC on the changes in (a) *BW*, (b) *GWF*, and (c) *GWS* in DRB during 1970 to 2017.

Under the coupled influences of climate change and LUCC, the *BW* and *GW* resources in DRB have changed. However, there were differences in the joint impacts of climate change and

LUCC on *BW* and *GW*. Both climate change and LUCC have led to the decrease of *BW* in the watershed, and the combined effect of climate change and LUCC on *BW* equals to the sum of their individual effects. Climate change, such as a decrease in potential evapotranspiration, has resulted in a decrease in *GWF* in DRB, while LUCC has led to an increase in *GWF*. Therefore, the joint impacts of climate change and LUCC on *GWF* was partially offset, resulting in the joint impacts of climate change and LUCC on *GWF* being less than the sum of their absolute individual effects. Both climate change and LUCC have led to an increase in *GWS* in DRB, and the joint impacts of climate change and LUCC on *GWS* equals to the sum of their individual effects.

4 Discussion

This study used the SWAT model to simulate the changes in *BW* and *GW* resources in DRB over the past five decades and their response to climate change and LUCC. It also assessed the water resource security in the basin. The findings revealed that the *GWF* exhibited a decreasing trend, and the *BW* and *GWS* exhibited an increasing trend. Liu et al. (2010) similarly found an increasing trend in annual surface runoff in DRB. Potential evapotranspiration in DRB showed a decreasing trend, which may be the main cause of the significant decrease in *GWF* in the basin (Fig. S3), and similar conclusions are obtained in He et al. (2013).

We show that water resources in DRB are dominated by *BW*, with a mean annual *GWI* of 0.4, which is the same as what many studies show in humid areas (Nie et al., 2023). Although the *GWI* in humid areas is much smaller than that in arid areas, the ratio of *GW* in DRB still reaches 40%, so it is imperative to incorporate *GW* in the water resources assessment system. The *GWI* in the upper and middle reaches of DRB exceeded 0.4, while that in the lower reaches was only about 0.3. These results mean that to ensure the appropriate utilization of water resources, effective water management in the upper and middle reaches of DRB should consider *GW* planning while water management in the lower reaches should mainly consider *BW*. The assessment results of *BWSC* and *GWSC* in DRB similarly illustrate this issue. The *GWSC* in the upper and middle reaches was bigger than that in the lower reaches of DRB, while the *BWSC* in the lower reaches of DRB was bigger than in the upper and middle reaches (Fig. 8).

There are robust correlations between *BW* and precipitation, *GWF* and potential evapotranspiration in DRB. Climate change plays a dominant role in variations of *BW* and *GWF*. *BW* is more sensitive to precipitation and potential evapotranspiration. *GWF* shows sensitivity to changes in potential evapotranspiration and *GWS* is influenced by both precipitation and potential evapotranspiration (He et al., 2015; Jeyrani et al., 2021). Of course, some studies in arid regions show that *GWF* is mainly affected by precipitation (Jun Wu et al., 2021), which may be linked to the hydrothermal conditions of the basin. There is sufficient precipitation in DRB, where the *GWF* changes are mainly energy-limited, and the effect of precipitation on the *GWF* is smaller.

Although *BW* and *GW* are mainly affected by climate change, the influences of LUCC on them cannot be ignored. The reaction of water resources to LUCC is exceedingly intricate and involves various hydrological processes, including runoff yield, infiltration, and groundwater (Cuo, 2016; Zhang and Shangguan, 2016). As there is a strong compensatory effect of diverse land use in the hydrological system, particularly in expansive watersheds, this could create a strong resistance to GW and BW conversion (Lin et al., 2015). A decrease in forest land or an increase in cultivated and urban land could lead to a rise in BW and a decline in GW in the watershed. Veettil and Mishra (2018) demonstrate that there is a 10% rise in forest land cover and a 1.4% drop in BW, indicating a negative elasticity between the two. However, the effect of urban land on streamflow in different periods showed the opposite effect. On the one hand, the increase in urban land results in increases in impermeable area and thus surface runoff in the basin, but at the same time, the increase in urban land may also reduce groundwater discharge to streamflow. At the same time, LUCC often results in changes in vegetation. Vegetation variations affect the water cycle by altering canopy interception (Shao et al., 2018; Jianping Wu et al., 2019), transpiration (Chen et al., 2023) and canopy evaporation, and ameliorating soil structure (Qiu et al., 2022), Thus increasing vegetation often increases infiltration and soil moisture and reduces surface runoff.

There are several limitations and uncertainties in this research. (1) Since the quantity of the BW and GW is derived from the output results of the model simulations, including water yield, ET, soil moisture, and groundwater, the precision of the outcomes depends largely on the precision of the model simulations. Given the absence of observed evapotranspiration and soil moisture data for DRB, this study calibrated and validated the SWAT model using only monthly streamflow, which may weaken these results to some extent. To enhance the credibility of the model, this study also utilized widely used actual evapotranspiration data (GLEAM) and soil moisture (ERA5-land) during model validation at a basin scale. The findings indicated that the simulation performance is relatively good and meets the accuracy requirements for simulation. (2) Climate change, LUCC, and large reservoir operation are the primary factors influencing the changes in hydrological conditions in DRB. The contributions of reservoir regulation, LUCC, water resource utilization, and climate change to the distribution of intra-annual flow are 33.5%, -9%, 4.5%, and 1%, respectively, during 1956-2009 (Tu et al., 2015). The operation of reservoirs, including large reservoirs like the Xinfengjiang Reservoir, is one of the important reasons for hydrological changes in DRB (Lin et al., 2014; Zhang et al., 2015). The reservoir module was not established when constructing the SWAT model in this research. To obtain natural *BW* and *GW* volumes in the watershed and mitigate the impact of hydraulic engineering, reconstructed natural streamflow based on observed flow was utilized for model calibration and validation. However, hydraulic engineering significantly influences the annual allocation of *BW*. The flow restoration considered the impacts of the three major reservoirs on the Dongjiang River and did not consider the impacts of other minor hydraulic projects and human water consumption. (3) Both the calculations of *BWSC* and the *FLK* index include environmental flows. This study represented the proportion of environmental flow in streamflow as 80%. Some studies have suggested that assuming environmental flow to be 80% of the total water resources in a basin may overestimate water scarcity (Liu et al., 2017; Richter et al., 2012). Therefore, we varied the proportion of environmental flow and assessed the degree of *BWSC* using 60% and 70% proportions. Results show that only the 63rd sub-basin changed from severe *BWSC* to moderate to high *BWSC*, while other sub-basins remained with low *BWSC*. Therefore, the threshold for environmental flow has a minor impact on this paper. The assessment of *BWSC* and per capita water resources did not take into account the water demand of cities such as Shenzhen and Hong Kong, although the water supply for these cities primarily comes from the Dongjiang River through the Dongjiang-Shenzhen Water Supply Project. (4) The hydrological modeling approach utilized in this research is a frequently used method for quantitative analysis of attribution. Nevertheless, it implies independence between climate change and LUCC and does not adequately distinguish the impacts of these two components. Such restriction is diffusely recognized to exist (Dey and Mishra, 2017). Despite this recognized limitation, hydrological modeling methods have been widely used in numerous similar researches, yielding credible results (Li et al., 2021; Nie et al., 2023).

5 Conclusion

This study analyzed the spatio-temporal evolution of *BW* and *GW*, assessed the water security, and evaluated the effects of climate change and LUCC on *BW* and *GW* in DRB using the SWAT model. The conclusions can be outlined as follows:

(1) During 1970-2017, grassland, cultivated land, and forestland in DRB decreased by 4.3%,

10.8%, and 0.2%, respectively, while urban land and water areas increased by 137% and 2.8%, respectively. The annual precipitation and potential evapotranspiration showed a non-significant decreasing trend, while the annual average temperature showed a significantly increasing trend.

(2) The annual *BW*, *GWF*, and green storage in DRB from 1970-2017 were 1240.8 mm, 840.7 mm, and 151.4mm, respectively. *BW* (0.14 mm a^{-1}) and *GWS* (0.015 mm a^{-1}) in DRB showed no significant increasing trend, and *GWF* (-0.57 mm a^{-1}) showed a significant decreasing trend.

(3) The level of annual *BWSC* and *GWSC* in DRB were low, and per capita water resources exceeded 1,700 m^3 $capita^{-1}$ a^{-1}. *BWSC* displayed a non-significant increasing trend, while the *GWSC* and *FLK* index displayed a significant decreasing trend, especially in lower reaches.

(4) Climate change was the major driving factor of changes in *BW* and *GWF*, and LUCC was the major driving factor of *GWS* change. Climate change contributed to 88.0%, 88.5%, and 39.4% of the changes in *BW*, *GWF*, and *GWS* in DRB, respectively. Both climate change and LUCC decrease (increase) *BW* (*GWS*), while climate change (LUCC) decreases (increases) *GWF* in DRB.

Competing interests

The contact author has declared that none of the authors has any competing interests.

Acknowledgments

This study was supported by the National Key Research and Development Program of China (2021YFC3001000), the Science and Technology Innovation Program from Water Resources of

Guangdong Province (2023-01), and the National Natural Science Foundation of China (52179029, 52179030).

References

Acero Triana, J.S., Ajami, H., 2022. Identifying Major Hydrologic Change Drivers in a Highly Managed Transboundary Endorheic Basin: Integrating Hydro-Ecological Models and Time Series Data Mining Techniques. Water Resources Research 58, e2022WR032281. https://doi.org/10.1029/2022WR032281

Aghakhani Afshar, A., Hassanzadeh, Y., Pourreza-Bilondi, M., Ahmadi, A., 2018. Analyzing long-term spatial variability of blue and green water footprints in a semi-arid mountainous basin with MIROC-ESM model (case study: Kashafrood River Basin, Iran). Theoretical and Applied Climatology 134, 885–899. https://doi.org/10.1007/s00704-017-2309-0

Arnold, J.G., Srinivasan, R., Muttiah, R.S., Williams, J.R., 1998. Large Area Hydrologic Modeling and Assessment Part I: Model Development1. JAWRA Journal of the American Water Resources Association 34, 73–89. https://doi.org/10.1111/j.1752-1688.1998.tb05961.x

Arshad, A., Mirchi, A., Samimi, M., Ahmad, B., 2022. Combining downscaled-GRACE data with SWAT to improve the estimation of groundwater storage and depletion variations in the Irrigated Indus Basin (IIB). Science of The Total Environment 838, 156044. https://doi.org/10.1016/j.scitotenv.2022.156044

Bai, X., Jia, X., Jia, Y., Shao, M., Hu, W., 2020. Modeling long-term soil water dynamics in response to land-use change in a semi-arid area. Journal of Hydrology 585, 124824. https://doi.org/10.1016/j.jhydrol.2020.124824

Berezovskaya, S., Yang, D., Kane, D.L., 2004. Compatibility analysis of precipitation and runoff trends over the large Siberian watersheds. Geophysical Research Letters 31. https://doi.org/10.1029/2004GL021277

Chagas, V.B.P., Chaffe, P.L.B., Blöschl, G., 2022. Climate and land management accelerate the Brazilian water cycle. Nat Commun 13, 5136. https://doi.org/10.1038/s41467-022-32580-x

Chen, Z., Wang, W., Cescatti, A., Forzieri, G., 2023. Climate-driven vegetation greening further reduces water availability in drylands. Global Change Biology 29, 1628–1647. https://doi.org/10.1111/gcb.16561

Chouchane, H., Krol, M.S., Hoekstra, A.Y., 2020. Changing global cropping patterns to minimize national blue water scarcity. Hydrology and Earth System Sciences 24, 3015–3031. https://doi.org/10.5194/hess-24-3015-2020

Cook, B.I., Smerdon, J.E., Seager, R., Coats, S., 2014. Global warming and 21 st century drying. Climate Dynamics 43, 2607–2627. https://doi.org/10.1007/s00382-014-2075-y

Cooper, C.M., Troutman, J.P., Awal, R., Habibi, H., Fares, A., 2022. Climate change-induced variations in blue and green water usage in U.S. urban agriculture. Journal of Cleaner Production 348, 131326. https://doi.org/10.1016/j.jclepro.2022.131326

Cuo, L., 2016. Land use/cover change impacts on hydrology in large river basins: a review. Terrestrial Water Cycle and Climate Change: Natural and Human-Induced Impacts 221, 103.

https://doi.org/10.1002/9781118971772.ch6
Dai, C., Qin, X., Dong, F., Cai, Y., 2022. Climate change impact on blue and green water resources distributions in the Beijiang River basin based on CORDEX projections. Journal of Water and Climate Change 13, 2780–2798. https://doi.org/10.2166/wcc.2022.115
Dey, P., Mishra, A., 2017. Separating the impacts of climate change and human activities on streamflow: A review of methodologies and critical assumptions. Journal of Hydrology 548, 278–290. https://doi.org/10.1016/j.jhydrol.2017.03.014
Ding, B., Zhang, J., Zheng, P., Li, Z., Wang, Y., Jia, G., Yu, X., 2024. Water security assessment for effective water resource management based on multi-temporal blue and green water footprints. Journal of Hydrology 632, 130761. https://doi.org/10.1016/j.jhydrol.2024.130761
Eekhout, J.P.C., Hunink, J.E., Terink, W., de Vente, J., 2018. Why increased extreme precipitation under climate change negatively affects water security. Hydrology and Earth System Sciences 22, 5935–5946. https://doi.org/10.5194/hess-22-5935-2018
Falkenmark, M., Folke, C., Falkenmark, Malin, 2003. Freshwater as shared between society and ecosystems: from divided approaches to integrated challenges. Philosophical Transactions of the Royal Society of London. Series B: Biological Sciences 358, 2037–2049. https://doi.org/10.1098/rstb.2003.1386
Falkenmark, M., Lundqvist, J., Widstrand, C., 1989. Macro-scale water scarcity requires micro-scale approaches. Natural Resources Forum 13, 258–267. https://doi.org/10.1111/j.1477-8947.1989.tb00348.x
Falkenmark, M., Rockström, J., 2006. The New Blue and Green Water Paradigm: Breaking New Ground for Water Resources Planning and Management. Journal of Water Resources Planning and Management 132, 129–132. https://doi.org/10.1061/(ASCE)0733-9496(2006)132:3(129)
Farr, T.G., Rosen, P.A., Caro, E., Crippen, R., Duren, R., Hensley, S., Kobrick, M., Paller, M., Rodriguez, E., Roth, L., Seal, D., Shaffer, S., Shimada, J., Umland, J., Werner, M., Oskin, M., Burbank, D., Alsdorf, D., 2007. The Shuttle Radar Topography Mission. Reviews of Geophysics 45. https://doi.org/10.1029/2005RG000183
Ficklin, D.L., Robeson, S.M., Knouft, J.H., 2016. Impacts of recent climate change on trends in baseflow and stormflow in United States watersheds. Geophys Res Lett 43, 5079–5088. https://doi.org/10.1002/2016gl069121
Fischer, G., Nachtergaele, F., Prieler, S., Van Velthuizen, H.T., Verelst, L., Wiberg, D., 2008. Global agro-ecological zones assessment for agriculture (GAEZ 2008). IIASA, Laxenburg, Austria and FAO, Rome, Italy 10.
Foley, J.A., DeFries, R., Asner, G.P., Barford, C., Bonan, G., Carpenter, S.R., Chapin, F.S., Coe, M.T., Daily, G.C., Gibbs, H.K., 2005. Global consequences of land use. Science 309, 570–574. https://doi.org/10.1126/science.1111772
Han, Z., Huang, S., Huang, Q., Bai, Q., Leng, G., Wang, H., Zhao, J., Wei, X., Zheng, X., 2020. Effects of vegetation restoration on groundwater drought in the Loess Plateau, China. Journal of Hydrology 591, 125566. https://doi.org/10.1016/j.jhydrol.2020.125566
He, Y., Lin, K., Chen, X., 2013. Effect of Land Use and Climate Change on Runoff in the Dongjiang Basin of South China. Mathematical Problems in Engineering 2013, e471429.

https://doi.org/10.1155/2013/471429
He, Y., Lin, K., Chen, X., Ye, C., Cheng, L., 2015. Classification-Based Spatiotemporal Variations of Pan Evaporation Across the Guangdong Province, South China. Water Resour Manage 29, 901–912. https://doi.org/10.1007/s11269-014-0850-5
Hoek van Dijke, A.J., Herold, M., Mallick, K., Benedict, I., Machwitz, M., Schlerf, M., Pranindita, A., Theeuwen, J.J.E., Bastin, J.-F., Teuling, A.J., 2022. Shifts in regional water availability due to global tree restoration. Nature Geoscience 15, 363–368. https://doi.org/10.1038/s41561-022-00935-0
Hoekstra, A.Y., Mekonnen, M.M., Chapagain, A.K., Mathews, R.E., Richter, B.D., 2012. Global Monthly Water Scarcity: Blue Water Footprints versus Blue Water Availability. PLOS ONE 7, e32688. https://doi.org/10.1371/journal.pone.0032688
Honrado, J.P., Vieira, C., Soares, C., Monteiro, M.B., Marcos, B., Pereira, H.M., Partidário, M.R., 2013. Can we infer about ecosystem services from EIA and SEA practice? A framework for analysis and examples from Portugal. Environmental Impact Assessment Review, Ecosystem services in EIA and SEA 40, 14–24. https://doi.org/10.1016/j.eiar.2012.12.002
Hordofa, A.T., Leta, O.T., Alamirew, T., Chukalla, A.D., 2023. Climate Change Impacts on Blue and Green Water of Meki River Sub-Basin. Water Resour Manage 37, 2835–2851. https://doi.org/10.1007/s11269-023-03490-4
Huang, H., Xue, Y., Chilukoti, N., Liu, Y., Chen, G., Diallo, I., 2020. Assessing Global and Regional Effects of Reconstructed Land-Use and Land-Cover Change on Climate since 1950 Using a Coupled Land–Atmosphere–Ocean Model. Journal of Climate 33, 8997–9013. https://doi.org/10.1175/JCLI-D-20-0108.1
Huang, Y., Cai, Y., Xie, Y., Zhang, F., He, Y., Zhang, P., Li, Bowen, Li, Bo, Jia, Q., Wang, Y., Qi, Z., 2022. An optimization model for water resources allocation in Dongjiang River Basin of Guangdong-Hong Kong-Macao Greater Bay Area under multiple complexities. Science of The Total Environment 820, 153198. https://doi.org/10.1016/j.scitotenv.2022.153198
Jeyrani, F., Morid, S., Srinivasan, R., 2021. Assessing basin blue–green available water components under different management and climate scenarios using SWAT. Agricultural Water Management 256, 107074. https://doi.org/10.1016/j.agwat.2021.107074
Jiang, J., Wang, Z., Lai, C., Wu, X., Chen, X., 2023. Climate and landuse change enhance spatio-temporal variability of Dongjiang river flow and ammonia nitrogen. Science of The Total Environment 867, 161483. https://doi.org/10.1016/j.scitotenv.2023.161483
Konapala, G., Mishra, A.K., Wada, Y., Mann, M.E., 2020. Climate change will affect global water availability through compounding changes in seasonal precipitation and evaporation. Nat Commun 11, 3044. https://doi.org/10.1038/s41467-020-16757-w
Lee, X., Goulden, M.L., Hollinger, D.Y., Barr, A., Black, T.A., Bohrer, G., Bracho, R., Drake, B., Goldstein, A., Gu, L., 2011. Observed increase in local cooling effect of deforestation at higher latitudes. Nature 479, 384–387. https://doi.org/10.1038/nature10588
Li, C., Tang, G., Hong, Y., 2018. Cross-evaluation of ground-based, multi-satellite and reanalysis precipitation products: Applicability of the Triple Collocation method across Mainland China. Journal of Hydrology 562, 71–83. https://doi.org/10.1016/j.jhydrol.2018.04.039

Li, X., Zhang, Y., Ma, N., Li, C., Luan, J., 2021. Contrasting effects of climate and LULC change on blue water resources at varying temporal and spatial scales. Science of The Total Environment 786, 147488. https://doi.org/10.1016/j.scitotenv.2021.147488

Lian, X., Piao, S., Li, L.Z.X., Li, Y., Huntingford, C., Ciais, P., Cescatti, A., Janssens, I.A., Peñuelas, J., Buermann, W., Chen, A., Li, X., Myneni, R.B., Wang, X., Wang, Y., Yang, Y., Zeng, Z., Zhang, Y., McVicar, T.R., 2020. Summer soil drying exacerbated by earlier spring greening of northern vegetation. Science Advances 6, eaax0255. https://doi.org/10.1126/sciadv.aax0255

Liang, J., He, X., Zeng, G., Zhong, M., Gao, X., Li, Xin, Li, Xiaodong, Wu, H., Feng, C., Xing, W., 2018. Integrating priority areas and ecological corridors into national network for conservation planning in China. Science of the Total Environment 626, 22–29.

Liang, J., Liu, Q., Zhang, H., Li, Xiaodong, Qian, Z., Lei, M., Li, Xin, Peng, Y., Li, S., Zeng, G., 2020. Interactive effects of climate variability and human activities on blue and green water scarcity in rapidly developing watershed. Journal of Cleaner Production 265, 121834. https://doi.org/10.1016/j.jclepro.2020.121834

Lin, B., Chen, X., Yao, H., Chen, Y., Liu, M., Gao, L., James, A., 2015. Analyses of landuse change impacts on catchment runoff using different time indicators based on SWAT model. Ecological Indicators 58, 55–63. https://doi.org/10.1016/j.ecolind.2015.05.031

Lin, K., Lian, Y., Chen, X., Lu, F., 2014. Changes in runoff and eco-flow in the Dongjiang River of the Pearl River Basin, China. Front. Earth Sci. 8, 547–557. https://doi.org/10.1007/s11707-014-0434-y

Liu, B., Peng, S., Liao, Y., Long, W., 2018. The causes and impacts of water resources crises in the Pearl River Delta. Journal of Cleaner Production 177, 413–425. https://doi.org/10.1016/j.jclepro.2017.12.203

Liu, D., Chen, X., Lian, Y., Lou, Z., 2010. Impacts of climate change and human activities on surface runoff in the Dongjiang River basin of China. Hydrological Processes 24, 1487–1495. https://doi.org/10.1002/hyp.7609

Liu, J., Yang, H., Gosling, S.N., Kummu, M., Flörke, M., Pfister, S., Hanasaki, N., Wada, Y., Zhang, X., Zheng, C., Alcamo, J., Oki, T., 2017. Water scarcity assessments in the past, present, and future. Earth's Future 5, 545–559. https://doi.org/10.1002/2016EF000518

Liu, M., Wang, D., Chen, X., Chen, Y., Gao, L., Deng, H., 2022. Impacts of climate variability and land use on the blue and green water resources in a subtropical basin of China. Sci Rep 12, 20993. https://doi.org/10.1038/s41598-022-21880-3

Liu, M., Zhang, P., Cai, Y., Chu, J., Li, Y., Wang, X., Li, C., Liu, Q., 2023. Spatial-temporal heterogeneity analysis of blue and green water resources for Poyang Lake basin, China. Journal of Hydrology 617, 128983. https://doi.org/10.1016/j.jhydrol.2022.128983

Martens, B., Miralles, D.G., Lievens, H., Fernández-Prieto, D., Beck, H.E., Dorigo, W.A., Verhoest, N.E.C., 2017. GLEAM v3: satellite-based land evaporation and root-zone soil moisture. Geoscientific Model Development 10, 1903–1925. https://doi.org/10.5194/gmd-10-1903-2017

Martínez-Salvador, A., Conesa-García, C., 2020. Suitability of the SWAT Model for Simulating

Water Discharge and Sediment Load in a Karst Watershed of the Semiarid Mediterranean Basin. Water Resour Manage 34, 785–802. https://doi.org/10.1007/s11269-019-02477-4
Mohan, M., Kandya, A., 2015. Impact of urbanization and land-use/land-cover change on diurnal temperature range: A case study of tropical urban airshed of India using remote sensing data. Science of the Total Environment 506, 453–465. https://doi.org/10.1016/j.scitotenv.2014.11.006
Muñoz Sabater, J., 2019. ERA5-Land monthly averaged data from 1981 to present, Copernicus Climate Change Service (C3S) Climate Data Store (CDS).
Nearing, M.A., Jetten, V., Baffaut, C., Cerdan, O., Couturier, A., Hernandez, M., Le Bissonnais, Y., Nichols, M.H., Nunes, J.P., Renschler, C.S., 2005. Modeling response of soil erosion and runoff to changes in precipitation and cover. CATENA 61, 131–154. https://doi.org/10.1016/j.catena.2005.03.007
Neitsch, S., Arnold, J., Kiniry, J., Williams, J., King, K., 2002. Soil and water assessment tool (SWAT): theoretical documentation, version 2000. Texas Water Resources Institute, College Station, Texas, TWRI Report TR-191.
Nie, N., Li, T., Miao, Y., Zhang, W., Gao, H., He, H., Zhao, D., Liu, M., 2023. Asymmetry of blue and green water changes in the Yangtze river basin, China, examined by multi-water-variable calibrated SWAT model. Journal of Hydrology 625, 130099. https://doi.org/10.1016/j.jhydrol.2023.130099
Pandey, B.K., Khare, D., Kawasaki, A., Mishra, P.K., 2019. Climate Change Impact Assessment on Blue and Green Water by Coupling of Representative CMIP5 Climate Models with Physical Based Hydrological Model. Water Resour Manage 33, 141–158. https://doi.org/10.1007/s11269-018-2093-3
Pokhrel, Y., Felfelani, F., Satoh, Y., Boulange, J., Burek, P., Gädeke, A., Gerten, D., Gosling, S.N., Grillakis, M., Gudmundsson, L., Hanasaki, N., Kim, H., Koutroulis, A., Liu, J., Papadimitriou, L., Schewe, J., Müller Schmied, H., Stacke, T., Telteu, C.-E., Thiery, W., Veldkamp, T., Zhao, F., Wada, Y., 2021. Global terrestrial water storage and drought severity under climate change. Nat. Clim. Chang. 11, 226–233. https://doi.org/10.1038/s41558-020-00972-w
Qiu, D., Xu, R., Wu, C., Mu, X., Zhao, G., Gao, P., 2023. Effects of vegetation restoration on soil infiltrability and preferential flow in hilly gully areas of the Loess Plateau, China. CATENA 221, 106770. https://doi.org/10.1016/j.catena.2022.106770
Qiu, D., Xu, R., Wu, C., Mu, X., Zhao, G., Gao, P., 2022. Vegetation restoration improves soil hydrological properties by regulating soil physicochemical properties in the Loess Plateau, China. Journal of Hydrology 609, 127730. https://doi.org/10.1016/j.jhydrol.2022.127730
Richter, B.D., 2010. Re-thinking environmental flows: from allocations and reserves to sustainability boundaries. River Research and Applications 26, 1052–1063. https://doi.org/10.1002/rra.1320
Richter, B.D., Davis, M.M., Apse, C., Konrad, C., 2012. A Presumptive Standard for Environmental Flow Protection. River Research and Applications 28, 1312–1321. https://doi.org/10.1002/rra.1511
Schewe, J., Heinke, J., Gerten, D., Haddeland, I., Arnell, N.W., Clark, D.B., Dankers, R., Eisner,

S., Fekete, B.M., Colón-González, F.J., Gosling, S.N., Kim, H., Liu, X., Masaki, Y., Portmann, F.T., Satoh, Y., Stacke, T., Tang, Q., Wada, Y., Wisser, D., Albrecht, T., Frieler, K., Piontek, F., Warszawski, L., Kabat, P., 2014. Multimodel assessment of water scarcity under climate change. Proceedings of the National Academy of Sciences 111, 3245–3250. https://doi.org/10.1073/pnas.1222460110

Schuol, J., Abbaspour, K.C., Yang, H., Srinivasan, R., Zehnder, A.J., 2008. Modeling blue and green water availability in Africa. Water resources research 44.

Schyns, J.F., Hoekstra, A.Y., Booij, M.J., Hogeboom, R.J., Mekonnen, M.M., 2019. Limits to the world's green water resources for food, feed, fiber, timber, and bioenergy. Proceedings of the National Academy of Sciences 116, 4893–4898. https://doi.org/10.1073/pnas.1817380116

Shao, M., Wang, Y., Xia, Y., Jia, X., 2018. Soil drought and water carrying capacity for vegetation in the critical zone of the Loess Plateau: A review. Vadose Zone Journal 17, 1539–1663. https://doi.org/10.2136/vzj2017.04.0077

Sharma, A., Patel, P.L., Sharma, P.J., 2023. Blue and green water accounting for climate change adaptation in a water scarce river basin. Journal of Cleaner Production 426, 139206. https://doi.org/10.1016/j.jclepro.2023.139206

Shen, Q., Cong, Z., Lei, H., 2017. Evaluating the impact of climate and underlying surface change on runoff within the Budyko framework: A study across 224 catchments in China. Journal of Hydrology 554, 251–262. https://doi.org/10.1016/j.jhydrol.2017.09.023

Sherwood, S., Fu, Q., 2014. A drier future? Science 343, 737–739. https://doi.org/10.1126/science.1247620

Stocker, B.D., Tumber-Dávila, S.J., Konings, A.G., Anderson, M.C., Hain, C., Jackson, R.B., 2023. Global patterns of water storage in the rooting zones of vegetation. Nat. Geosci. 1–7. https://doi.org/10.1038/s41561-023-01125-2

Suzuki, K., Park, H., Makarieva, O., Kanamori, H., Hori, M., Matsuo, K., Matsumura, S., Nesterova, N., Hiyama, T., 2021. Effect of Permafrost Thawing on Discharge of the Kolyma River, Northeastern Siberia. Remote Sensing 13, 4389. https://doi.org/10.3390/rs13214389

Tan, X., Gan, T.Y., 2015. Contribution of human and climate change impacts to changes in streamflow of Canada. Sci Rep 5, 17767. https://doi.org/10.1038/srep17767

Tan, Xuezhi, Wu, X., Huang, Z., Deng, S., Hu, M., Yew Gan, T., 2022. Detection and attribution of the decreasing precipitation and extreme drought 2020 in southeastern China. Journal of Hydrology 610, 127996. https://doi.org/10.1016/j.jhydrol.2022.127996

Tan, Xuejin, Liu, B., Tan, Xuezhi, 2020. Global Changes in Baseflow Under the Impacts of Changing Climate and Vegetation. Water Resources Research 56, e2020WR027349. https://doi.org/10.1029/2020WR027349

Tan, Xuejin, Liu, B., Tan, Xuezhi, Chen, X., 2022. Long-Term Water Imbalances of Watersheds Resulting From Biases in Hydroclimatic Data Sets for Water Budget Analyses. Water Resources Research 58, e2021WR031209. https://doi.org/10.1029/2021WR031209

Tan, Xuejin, Tan, Xuezhi, Liu, B., Huang, Z., 2023. Contribution of changes in vegetation composition and climate variability on streamflow across the global watersheds. CATENA 232, 107394. https://doi.org/10.1016/j.catena.2023.107394

Tao, S., Fang, J., Ma, S., Cai, Q., Xiong, X., Tian, D., Zhao, X., Fang, L., Zhang, H., Zhu, J., Zhao, S., 2020. Changes in China's lakes: climate and human impacts. National Science Review 7, 132–140. https://doi.org/10.1093/nsr/nwz103

Tu, X., Singh, V.P., Chen, X., Chen, L., Zhang, Q., Zhao, Y., 2015. Intra-annual Distribution of Streamflow and Individual Impacts of Climate Change and Human Activities in the Dongijang River Basin, China. Water Resour Manage 29, 2677–2695. https://doi.org/10.1007/s11269-015-0963-5

Tu, X., Wu, H., Singh, V.P., Chen, X., Lin, K., Xie, Y., 2018. Multivariate design of socioeconomic drought and impact of water reservoirs. Journal of Hydrology 566, 192–204. https://doi.org/10.1016/j.jhydrol.2018.09.012

Vano, J.A., Das, T., Lettenmaier, D.P., 2012. Hydrologic sensitivities of Colorado River runoff to changes in precipitation and temperature. Journal of Hydrometeorology 13, 932–949. https://doi.org/10.1175/JHM-D-11-069.1

Veettil, A.V., Mishra, A., 2020. Water Security Assessment for the Contiguous United States Using Water Footprint Concepts. Geophysical Research Letters 47, e2020GL087061. https://doi.org/10.1029/2020GL087061

Veettil, A.V., Mishra, A.K., 2018. Potential influence of climate and anthropogenic variables on water security using blue and green water scarcity, Falkenmark index, and freshwater provision indicator. Journal of Environmental Management 228, 346–362. https://doi.org/10.1016/j.jenvman.2018.09.012

Veettil, A.V., Mishra, A.K., 2016. Water security assessment using blue and green water footprint concepts. Journal of Hydrology 542, 589–602. https://doi.org/10.1016/j.jhydrol.2016.09.032

Walters, K.M., Babbar-Sebens, M., 2016. Using climate change scenarios to evaluate future effectiveness of potential wetlands in mitigating high flows in a Midwestern US watershed. Ecological engineering 89, 80–102. https://doi.org/10.1016/j.ecoleng.2016.01.014

Wu, Jiefeng, Chen, X., Yu, Z., Yao, H., Li, W., Zhang, D., 2019. Assessing the impact of human regulations on hydrological drought development and recovery based on a 'simulated-observed' comparison of the SWAT model. Journal of Hydrology 577, 123990. https://doi.org/10.1016/j.jhydrol.2019.123990

Wu, Jiefeng, Chen, X., Yuan, X., Yao, H., Zhao, Y., AghaKouchak, A., 2021. The interactions between hydrological drought evolution and precipitation-streamflow relationship. Journal of Hydrology 597, 126210. https://doi.org/10.1016/j.jhydrol.2021.126210

Wu, Jun, Deng, G., Zhou, D., Zhu, X., Ma, J., Cen, G., Jin, Y., Zhang, J., 2021. Effects of climate change and land-use changes on spatiotemporal distributions of blue water and green water in Ningxia, Northwest China. J. Arid Land 13, 674–687. https://doi.org/10.1007/s40333-021-0074-5

Wu, Jianping, Liu, L., Sun, C., Su, Y., Wang, C., Yang, J., Liao, J., He, X., Li, Q., Zhang, C., Zhang, H., 2019. Estimating Rainfall Interception of Vegetation Canopy from MODIS Imageries in Southern China. Remote Sensing 11, 2468. https://doi.org/10.3390/rs11212468

Xin, Z., Li, Y., Zhang, L., Ding, W., Ye, L., Wu, J., Zhang, C., 2019. Quantifying the relative contribution of climate and human impacts on seasonal streamflow. Journal of Hydrology

574, 936–945. https://doi.org/10.1016/j.jhydrol.2019.04.095
Xu, X., 2017. China population spatial distribution kilometer grid dataset. Data Registration and Publishing System of Resource and Environmental Science Data Center of Chinese Academy of Sciences.
Xu, X., Liu, J., Zhang, S., Li, R., Yan, C., Wu, S., 2018. Multi-period land use land cover remote sensing monitoring dataset in China (CNLUCC). Resource and Environmental Science Data Registration and Publication System. (http://www. resdc. cn/DOI). https://doi.org/DOI:10.12078/2018070201
Yang, L.E., Chan, F.K.S., Scheffran, J., 2018. Climate change, water management and stakeholder analysis in the Dongjiang River basin in South China. International Journal of Water Resources Development 34, 166–191. https://doi.org/10.1080/07900627.2016.1264294
Zang, C., Liu, J., 2013. Trend analysis for the flows of green and blue water in the Heihe River basin, northwestern China. Journal of Hydrology 502, 27–36. https://doi.org/10.1016/j.jhydrol.2013.08.022
Zhang, Q., Gu, X., Singh, V.P., Chen, X., 2015. Evaluation of ecological instream flow using multiple ecological indicators with consideration of hydrological alterations. Journal of Hydrology 529, 711–722. https://doi.org/10.1016/j.jhydrol.2015.08.066
Zhang, Y., Shangguan, Z., 2016. The change of soil water storage in three land use types after 10years on the Loess Plateau. CATENA 147, 87–95. https://doi.org/10.1016/j.catena.2016.06.036
Zhang, Yongyong, Xia, J., Yu, J., Randall, M., Zhang, Yichi, Zhao, T., Pan, X., Zhai, X., Shao, Q., 2018. Simulation and assessment of urbanization impacts on runoff metrics: insights from landuse changes. Journal of Hydrology 560, 247–258. https://doi.org/10.1016/j.jhydrol.2018.03.031
Zuo, D., Xu, Z., Peng, D., Song, J., Cheng, L., Wei, S., Abbaspour, K.C., Yang, H., 2015. Simulating spatiotemporal variability of blue and green water resources availability with uncertainty analysis. Hydrological Processes 29, 1942–1955.